Reversion of a parent {130}<310>$_{\alpha''}$ martensitic twinning system at the origin of {332}<113>$_{\beta}$ twins observed in metastable β titanium alloys

P. Castany[1,*], Y. Yang[1], E. Bertrand[2], T. Gloriant[1,*]

[1]*INSA de Rennes, UMR CNRS 6226 Institut des Sciences Chimiques de Rennes/Chimie-Métallurgie, 20 avenue des Buttes de Coësmes, 35708, Rennes, France*

[2]*Institut des Matériaux Jean Rouxel (IMN), Université de Nantes, CNRS, Rue Christian Pauc, 44306, Nantes, France*

In bcc metastable β titanium alloys, and particularly in superelastic alloys, a unique {332}<113> twinning system occurs during plastic deformation. However, *in situ* synchrotron X-ray diffraction during tensile test shows that β phase totally transforms into α" martensite under stress in a Ti-27Nb (at.%) alloy. {332}<113>$_{\beta}$ twins are thus not formed directly in β phase but are the resultant of the reversion of {130}<310>$_{\alpha''}$ parent twins occurring in martensite under stress. Formation of interfacial twin boundary ω phase is also observed to accommodate strains induced during the phase reversion.

[*]email: philippe.castany@insa-rennes.fr; thierry.gloriant@insa-rennes.fr

Metastable β titanium alloys are actually considered in various domains and more specifically for biomedical applications due to their unique properties combining high strength, low elastic modulus, excellent biocompatibility and potentially shape memory or superelastic properties depending on alloy compositions. The high temperature β phase (bcc) is thus obtained by addition of β-stabilizer elements (Nb, Ta, Mo…) and rapid quenching from the high temperature β-domain in order to retain it at room temperature in a metastable state. Deformation of these alloys can be accommodated by several deformation mechanisms such as stress-induced martensitic transformation [1-6], dislocation slip [7-10] and twinning [11-19]. While twinning in bcc metals and alloys operates normally with the {112}<111>$_{\beta}$ system, a unique {332}<113>$_{\beta}$ twinning system is surprisingly found to be predominant in

metastable β titanium alloys. Since its first identification in 1971 [20], the question why $\{332\}\langle 113\rangle_\beta$ twinning occurs in these alloys is still open. Indeed, the requirement of additional shuffle of atoms in addition to shear makes this twinning system energetically unfavorable in comparison with the $\{112\}\langle 111\rangle_\beta$ system that involves only shear [21]. Several models were proposed to describe its formation as a shear of β phase by partial dislocations along $\langle 113\rangle_\beta$ directions followed by necessary shuffles of atoms [13,22-24]. The difference among these models lies in the magnitude of partial dislocations and shuffles, but no explanation of the dominance of $\{332\}\langle 113\rangle_\beta$ twinning was given. More recently, a new model based on the description of β phase as a modulated structure containing base-centered tetragonal nanodomains shows that $\{332\}\langle 113\rangle_\beta$ twinning is more favorable [25]. However, nanodomains with such symmetry were never observed until now. It can also be noticed that such alloys can undergo a reversible stress-induced martensitic transformation from the β phase to a C-centered orthorhombic α" phase, leading to superelastic properties [1,2,4,26] or TRIP (transformation induced plasticity) effect [27,28] depending on alloy compositions. That is why the origin of $\{332\}\langle 113\rangle_\beta$ twinning was early suggested to be linked with this phase transformation but without more details about the mechanism involved [20]. The present letter aims to elucidate the role of stress-induced α" martensite in the formation of $\{332\}\langle 113\rangle_\beta$ twinning. To avoid any effect of complex chemical compositions, the binary Ti-27Nb (at.%) alloy was chosen for this study.

The Ti-27Nb alloy was elaborated by cold crucible levitation melting from pure raw metals (99,999% pure Ti and 99,9% pure Nb) leading to low oxygen content (150 ppm). Ingots were next homogenized at 1223 K during 20 hours, 90% cold rolled, recrystallized at 1143 K during 0.5 hour and water quenched. Loading-unloading cyclic tensile tests, composed of 0.5% strain increments followed by stress release, were performed on normalized specimens until an elongation of 5% with a 10^{-4} s^{-1} strain rate (tensile direction parallel to the rolling direction). Initial microstructure was characterized by optical microscopy and synchrotron X-ray diffraction (SXRD) using a 0.040002106 nm wavelength radiation. In order to characterize the microstructure under stress, *in situ* SXRD experiments were carried out at the high-resolution beam line ID31 of the European Synchrotron Radiation Facility (ESRF) in Grenoble (France). Diffraction patterns were recorded during interrupted tensile tests at different strain levels [4]. Microstructure after deformation was observed by electron backscattered diffraction (EBSD) in scanning electron microscopy (SEM) and by transmission electron microscopy (TEM) in tensile specimens after being strained up to 5%. EBSD specimens were mechanically polished followed by chemical etching and TEM

specimens were prepared using classical twin-jet electropolishing stopped before perforation and followed by ion milling.

The investigated Ti-27Nb alloy is only composed of β phase as shown on the SXRD pattern in Fig. 1(a). Its initial microstructure consists of equiaxial grains with size ranging between 50 and 100 μm [Fig. 1(b)]. The cyclic tensile test of the Fig. 1(c) confirms the superelastic behavior of this alloy: a stress plateau is clearly visible on the curve and a large reversibility of the strain can be observed during unloading. The superelasticity, i.e. the largest recoverable strain, is of 1.8% that is consistent with values reported for Ti-Nb based alloys with the same or similar compositions [1,29].

In order to determine the phase constitution during deformation, tensile tests were performed *in situ* under synchrotron X-ray radiation. Diffractograms were recorded at different steps during the test as displayed in Fig. 1(d). To ensure a better readability, diffractograms were focused on a small angular range around the main peak of β phase $(110)_{\beta}$. A small amount of α" martensite, formed during the quench, can be identified on the initial diffractogram as $(020)_{\alpha''}$ (white square) and $(111)_{\alpha''}$ peaks (white star). These peaks vanish progressively when the stress increases and have no particular influence as reported before [4]. However, when the stress increases, the intensity of the $(110)_{\beta}$ peak (black triangle) decreases continuously while $(020)_{\alpha''}$ (black square) and $(002)_{\alpha''}$ (black circle) peaks of stress-induced α" martensite appears. At 1% strain, $(110)_{\beta}$ and $(020)_{\alpha''}$ peaks exhibit approximately the same intensity. At 2% strain, the $(110)_{\beta}$ peak has nearly vanished and, from 3% strain, only peaks of α" martensite are detected. Initial lattice parameters of the β phase are calculated as a_{β}=0.3285 nm and the α" martensite ones as $a_{\alpha''}$=0.3225 nm, $b_{\alpha''}$=0.4780 nm and $c_{\alpha''}$=0.4682 nm from the diffractogram at 5% strain (under stress). These observations are consistent with the tensile curve in Fig. 1(c) and illustrate that the superelasticity is due to the β to α" stress-induced martensitic transformation. But the most important result is that from 3% strain, no more β phase is present in the microstructure that is fully composed of α" martensite under stress.

Twinning was first characterized from EBSD observations of specimens strained until 5%. An example is provided in Fig. 2, in which most of grains present large deformation bands of 5-10 μm width. EBSD data were indexed by the β phase indicating a full reverse transformation after releasing the stress. Consequently, all deformation bands were characterized as $\{332\}\langle 113\rangle_{\beta}$ twins since ~50° misorientation is measured between each parent grain and twin [14,29]. At finer scale, twins are observed by TEM. The Fig. 3(a) shows a typical bright-field TEM image wherein the twin interface is edge-on. The corresponding selected area

electron diffraction (SAED) pattern taken at the twin interface is provided in Fig. 3(b). For a better readability, SAED patterns for each crystal are indexed separately in Fig. 3(c) for the matrix and Fig. 3(d) for the twin. Both SAED patterns correspond to $<110>_{\beta}$ zone axis disorientated of 50.4°, that confirms the $\{332\}<113>_{\beta}$ type of the twin.

Both EBSD and TEM observations show thus only β phase after deformation with large occurrence of $\{332\}<113>_{\beta}$ twinning in the Ti-27Nb alloy, similarly to previous observations in various metastable titanium-based alloys [11-19,29]. However, *in situ* SXRD experiments show the microstructure is fully composed of α" from 3% strain [Fig. 1(d)]. As twinning occurs in the plastic domain, i.e. after the stress plateau on the tensile curve (after 2% strain), that means the β phase has totally transformed into α" when twinning is occurring and, consequently, the observed $\{332\}<113>_{\beta}$ twins are not really formed in β phase. Present experiments show thus unambiguously that twinning occurs in α" martensite and, when the stress is removed, the twinned martensite transforms back to β phase leading to a remnant deformation band corresponding to a $\{332\}<113>_{\beta}$ twinning relationship. One can wonder now which is the real twinning mechanism occurring under stress in α" martensite. Due to the reversibility of this transformation, twinning of stress-induced martensite in superelastic alloys was never reported. However, plastic twinning of α" martensite was rarely reported for full-α" Ti-based shape memory alloys after deformation: $<110>\{110\}_{\alpha''}$ twinning was observed only at the surface of tensile specimens [30] and $\{130\}<310>_{\alpha''}$ twinning system was observed to occur extensively in bulk material [31]. As the existence of other twinning systems in α" martensite cannot be excluded, we tried to determine which twinning system is occurring in α" martensite. Even if this phase is no more present to be directly observed, its crystallographic orientation can be determined by applying the well-known orientation relationship (OR) between β and α" phases [1,31]. By way of illustration, the crystallographic orientations of the parent grain (matrix) and the twin observed in Fig. 3 are first obtained from TEM data and represented on stereographic projections in Fig. 4(a-b). The corresponding orientations of matrix and twin after transformation into α" martensite are then determined by applying the OR. But, from one orientation of β phase, six possible orientations of α" phase, named variants, exist: As the variant actually formed is not known *a priori*, the six possible orientations for the matrix and the six ones for the twin were constructed. All the combinations between both crystals were finally tested in order to find a twinning relationship in α" phase. For that, common poles in both crystals are searched and, if there are, a rotation of 180° around them is made to confirm the twinning relationship (more details in ref. [31]). Fortunately, only one unique solution, corresponding to the $\{130\}<310>_{\alpha''}$ twinning system, is

systematically found as reported in Fig. 4, where the α" orientations of the matrix [Fig. 4(c)] and the twin [Fig. 4(d)] are represented with their common $\{130\}_{\alpha"}$ and $<310>_{\alpha"}$ poles. The sole possibility is thus that $\{130\}<310>_{\alpha"}$ twinning in α" stress-induced martensite occurs during deformation and transforms back to a deformation band with the $\{332\}<113>_{\beta}$ twinning relationship in β phase when the stress is removed. This scenario is possible because of the correspondence between both $\{130\}<310>_{\alpha"}$ and $\{332\}<113>_{\beta}$ twinning systems as shown in Fig. 4 and previously pointed out from theoretic considerations [31]. Similarly to the existence of parent phase and product phase in shape memory alloys, there is here parent twins, namely $\{130\}<310>_{\alpha"}$ in martensite, that transform to $\{332\}<113>_{\beta}$ product twins after reverse transformation when removing the stress.

However, the twin interface appears rather thick in bright-field TEM images even if the interface is edge-on [Fig. 3(e)] whereas a twin interface is expected to be one atomic layer thick due to its high coherency. Moreover, the diffraction pattern exhibits some extra spots with lower intensity than spots of β phase [Fig. 3(b)]. This spots are not present on diffraction patterns taken within twin and matrix [Fig. 3(c-d)]. The dark-field image of the Fig. 3(f), which is taken with the spot circled in Fig. 3(b), shows these spots are due to an additional phase present at the twin interface with a thickness of 15 nm. Its diffraction pattern can be indexed as a $<11\text{-}20>_{\omega}$ zone axis of a single variant of the hexagonal ω phase, with the circled spot of Fig. 3(b) corresponding to the $(0001)_{\omega}$ reflection. Lattice parameters can thus be determined as a_{ω}=0.448 nm and c_{ω}=0.274 nm. The ω phase is commonly found in metastable β titanium alloys as nanometric-sized precipitates formed after quenching or low-temperature ageing [1,32,33]. Stress-induced ω phase is also sometimes reported as fine laths in deformed specimens [17,27,33,34]. But such interfacial ω phase lying on twin boundaries was never reported before. However, unexpected interfacial phases were predicted to form in order to minimize the surface energy of boundaries [35,36]. Such intergranular films (IGF), also known as planar complexions, were observed in some materials [37,38]. The ω phase we observed here is thus a kind of IGF specifically located on twin boundaries, hereafter called interfacial twin boundary (ITB) ω phase. Formation of ITB ω phase is assumed to accommodate strains that are induced from the inverse martensitic transformation of $\{130\}<310>_{\alpha"}$ twin boundaries into $\{332\}<113>_{\beta}$ twin interfaces. The whole process of $\{332\}<113>_{\beta}$ twin formation is finally illustrated in Fig. 5: By increasing the applied strain, β phase transforms first in α" martensite that is further deformed by $\{130\}<310>_{\alpha"}$ twinning; when the stress is released, α" martensite transforms back to β phase leading to a product $\{332\}<113>_{\beta}$ twin bounded with ITB ω phase.

In addition, the OR between β and ω phases is found from Fig. 3(b) as: $\{113\}_\beta//(0001)_\omega$ and $<110>_\beta//<11\text{-}20>_\omega$. While the usual OR is known as: $\{111\}_\beta//(0001)_\omega$ and $<110>_\beta//<11\text{-}20>_\omega$ [33]. As a consequence, a $\{1\text{-}100\}_\omega$ plane is parallel to a $\{332\}_\beta$ plane instead of a $\{112\}_\beta$ plane. The correspondence between directions is unchanged, but the common plane is rotated of 90° around the common direction. Deviations from the regular OR, with unchanged common directions but different common planes, were sometimes observed for stress-induced ω plates [17,34]. It can also be noticed that the observed ITB ω phase seems in strong correlation with the twin interface as the $<113>_\beta$ twin direction is normal to the $<0001>_\omega$ direction and a $\{1\text{-}100\}_\omega$ plane is parallel to the $\{332\}_\beta$ twin plane. The classical mechanism of formation of ω phase, which involves the collapse of adjacent $\{111\}_\beta$ planes [33], cannot explain the observed OR and another mechanism has to be considered. The simplest pathway to obtain the present OR can be described as the collapse of two adjacent $\{332\}_\beta$ planes and a subsequent consecutive shear of atoms along the $<113>_\beta$ direction belonging to this resulting plane. The collapse of two adjacent $\{332\}_\beta$ planes corresponds thus exactly to a $\{1\text{-}100\}_\omega$ plane and the shuffle along the $<113>_\beta$ direction makes $\{113\}_\beta$ parallel to $(0001)_\omega$ as observed in Fig. 3(b). This new mechanism involving consecutive shear of atoms is similar to one already proposed for the formation of stress-induced ω phase [39]. This new OR is certainly imposed by the twin boundary because the collapsing $\{332\}_\beta$ planes correspond to the twin plane, which are the result of the reverse transformation of $\{130\}_{\alpha''}$ twin planes. This collapse can be explained from the mismatch between lattice spacing of the twin plane in both phases, which corresponds to a misfit of 1.98% in compression when the reverse transformation occurs (calculated from SXRD data). This compressive misfit can thus be a driving force to explain why the ω phase is formed by the collapse of $\{332\}_\beta$ planes instead of $\{111\}_\beta$ planes.

In the literature, $\{332\}<113>_\beta$ twins always exhibit features attributed to stress-relaxation phenomena, which were not clearly understood, such as large arrays of dislocations around twin boundaries [11-13,24], stress-induced preferential growth of nanometric-sized preexisting athermal ω phase [15], single variant ω plates inside twins [11,12] or ITB ω phase [present study]. As twins are formed in α" martensite, all these features can be interpreted as products of relaxation of strains due to mismatch of lattice parameters between α" and β phases during the reverse transformation. Indeed, as lattice parameters of α" martensite are strongly dependent on chemical composition [1], the misfit strain magnitude depends on alloy composition, which is, in turn, relaxed by different way (dislocation arrays, ω phase).

Occurrence of $\{332\}\langle 113\rangle_\beta$ twinning is also often related to the β phase stability and is observed in the less stable alloys while $\{112\}\langle 111\rangle_\beta$ twinning takes place in more stable ones [11,16,40]. This is in very good agreement with present results as the stress-induced martensitic transformation also occurs in the less stable alloys. One can first easily assume that $\{332\}\langle 113\rangle_\beta$ twinning is always formed from reversion of $\{130\}\langle 310\rangle_{\alpha''}$ twins in superelastic alloys, that are the less stable ones (like the present Ti-27Nb alloy). Secondly, when the β-stability increases, stress-induced martensitic transformation still occurs but not in a reversible manner and leads to TRIP effect: $\{332\}\langle 113\rangle_\beta$ twinning is thus most probably initiate as $\{130\}\langle 310\rangle_{\alpha''}$ twins and can propagate through the β phase as the mismatch in lattice parameters is smaller. Finally, in more stable alloys, there is no more stress-induced martensitic transformation to initiate $\{332\}\langle 113\rangle_\beta$ twinning, making the classical $\{112\}\langle 111\rangle_\beta$ twinning easier to form instead.

As a summary, the peculiar $\{332\}\langle 113\rangle_\beta$ twinning system observed in metastable β titanium alloys is shown to be the consequence of the reversion of a parent $\{130\}\langle 310\rangle_{\alpha''}$ twinning in stress-induced α" martensite. We evidenced that such parent twins are formed in α" martensite and lead to $\{332\}\langle 113\rangle_\beta$ product twins in β phase after reverse phase transformation when the applied stress is released. Moreover, stress relaxation occurs close to the twin boundary during the reverse phase transformation due to mismatch between lattice parameters and leads to specific features observed around $\{332\}\langle 113\rangle_\beta$ twins. Consequently, a new interfacial twin boundary (ITB) ω phase formation mechanism was highlighted at the twin boundaries in the present Ti-27Nb alloy. This new formation pathway of twins can also be potentially found in any materials exhibiting stress-induced phase transformation such as shape memory alloys, TRIP steels or some ceramics and thus help to elucidate unexplained features of some twinning systems.

The authors acknowledge the European Synchrotron Radiation Facility for provision of synchrotron radiation facilities and would like to thank Yves Watier for assistance in using the beamline ID31. The authors also acknowledge the THEMIS platform of the University of Rennes for providing access to TEM facilities.

[1] H. Y. Kim, Y. Ikehara, J. I. Kim, H. Hosoda, and S. Miyazaki, Acta Mater. **54**, 2419 (2006).
[2] M. Tahara, H. Y. Kim, H. Hosoda, and S. Miyazaki, Acta Mater. **57**, 2461 (2009).
[3] Y. Al-Zain, H. Y. Kim, T. Koyano, H. Hosoda, T. H. Nam, and S. Miyazaki, Acta Mater. **59**, 1464 (2011).
[4] P. Castany, A. Ramarolahy, F. Prima, P. Laheurte, C. Curfs, and T. Gloriant, Acta Mater. **88**, 102 (2015).
[5] Y. Yang, P. Castany, M. Cornen, F. Prima, S. J. Li, Y. L. Hao, and T. Gloriant, Acta Mater. **88**, 25 (2015).
[6] M. F. Ijaz, H. Y. Kim, H. Hosoda, and S. Miyazaki, Mater. Sci. Eng. C **48**, 11 (2015).
[7] P. Castany, M. Besse, and T. Gloriant, Scripta Mater. **66**, 371 (2012).
[8] P. Castany, M. Besse, and T. Gloriant, Phys. Rev. B **84**, 020201 (2011).
[9] M. J. Lai, C. C. Tasan, and D. Raabe, Acta Mater. **100**, 290 (2015).
[10] Y. Kamimura, S. Katakura, K. Edagawa, S. Takeuchi, S. Kuramoto, and T. Furuta, Mater. Trans. **56**, 2084 (2015).
[11] S. Hanada and O. Izumi, Metall. Trans. A **17**, 1409 (1986).
[12] T. Furuhara, K. Kishimoto, and T. Maki, Mater. Trans. **35**, 843 (1994).
[13] T. Kawabata, S. Kawasaki, and O. Izumi, Acta Mater. **46**, 2705 (1998).
[14] E. Bertrand, P. Castany, I. Péron, and T. Gloriant, Scripta Mater. **64**, 1110 (2011).
[15] X. Zhao, M. Niinomi, M. Nakai, G. Miyamoto, and T. Furuhara, Acta Biomater. **7**, 3230 (2011).
[16] M. Ahmed, D. Wexler, G. Casillas, O. M. Ivasishin, and E. V. Pereloma, Acta Mater. **84**, 124 (2015).
[17] X. L. Wang, L. Li, H. Xing, P. Ou, and J. Sun, Scripta Mater. **96**, 37 (2015).
[18] X. Min, X. Chen, S. Emura, and K. Tsuchiya, Scripta Mater. **69**, 393 (2013).
[19] H. Zhan, W. Zeng, G. Wang, D. Kent, and M. Dargusch, Scripta Mater. **107**, 34 (2015).
[20] M. J. Blackburn and J. A. Feeney, J. Inst. Met. **99**, 132 (1971).
[21] J. W. Christian and S. Mahajan, Prog. Mater. Sci. **39**, 1 (1995).
[22] A. G. Crocker, Acta Metall. **10**, 113 (1962).
[23] P. G. Oberson and S. Ankem, Phys. Rev. Lett. **95**, 165501 (2005).
[24] G. Rusakov, A. Litvinov, and V. Litvinov, Met. Sci. Heat Treat. **48**, 244 (2006).
[25] H. Tobe, H. Y. Kim, T. Inamura, H. Hosoda, and S. Miyazaki, Acta Mater. **64**, 345 (2014).
[26] Y. L. Hao, S. J. Li, S. Y. Sun, and R. Yang, Mater. Sci. Eng. A **441**, 112 (2006).
[27] F. Sun, et al., Acta Mater. **61**, 6406 (2013).

[28] M. Marteleur, F. Sun, T. Gloriant, P. Vermaut, P. J. Jacques, and F. Prima, Scripta Mater. **66**, 749 (2012).
[29] A. Ramarolahy, P. Castany, F. Prima, P. Laheurte, I. Péron, and T. Gloriant, J. Mech. Behav. Biomed. Mater. **9**, 83 (2012).
[30] D. H. Ping, Y. Yamabe-Mitarai, C. Y. Cui, F. X. Yin, and M. A. Choudhry, Appl. Phys. Lett. **93**, 151911 (2008).
[31] E. Bertrand, P. Castany, Y. Yang, E. Menou, and T. Gloriant, Acta Mater. **105**, 94 (2016).
[32] F. Sun, F. Prima, and T. Gloriant, Mater. Sci. Eng. A **527**, 4262 (2010).
[33] S. Banerjee, R. Tewari, and G. K. Dey, Int. J. Mater. Res. **97**, 963 (2006).
[34] T. S. Kuan, R. R. Ahrens, and S. L. Sass, Metall. Trans. A **6**, 1767 (1975).
[35] M. Tang, W. C. Carter, and R. M. Cannon, Phys. Rev. Lett. **97**, 075502 (2006).
[36] P. R. Cantwell, M. Tang, S. J. Dillon, J. Luo, G. S. Rohrer, and M. P. Harmer, Acta Mater. **62**, 1 (2014).
[37] M. Baram, D. Chatain, and W. D. Kaplan, Science **332**, 206 (2011).
[38] V. K. Gupta, D.-H. Yoon, H. M. Meyer III, and J. Luo, Acta Mater. **55**, 3131 (2007).
[39] L. M. Hsiung and D. H. Lassila, Acta Mater. **48**, 4851 (2000).
[40] M. Abdel-Hady, K. Hinoshita, and M. Morinaga, Scripta Mater. **55**, 477 (2006).

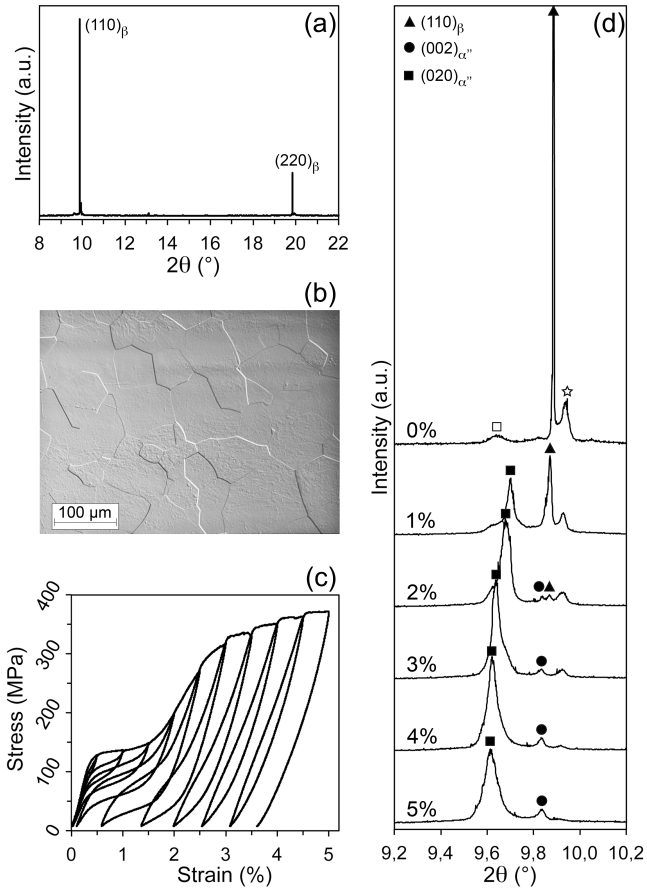


FIG. 1. Initial microstructure of the Ti-27Nb alloy: (a) SXRD pattern and (b) optical micrograph. (c) Cyclic tensile curve. (d) SXRD patterns taken under stress at different strains during *in situ* tensile test.

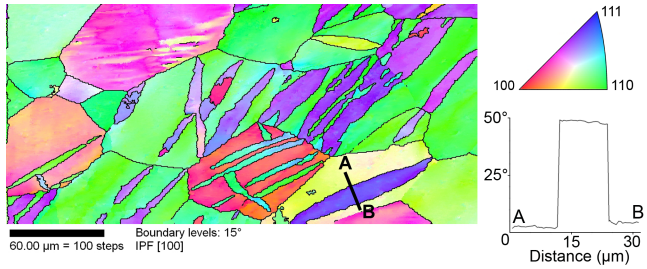


FIG. 2. EBSD inverse pole figure map after deformation presenting large bands identified as {332}<113>$_\beta$ twins (example of misorientation profile along the AB line crossing a twin).

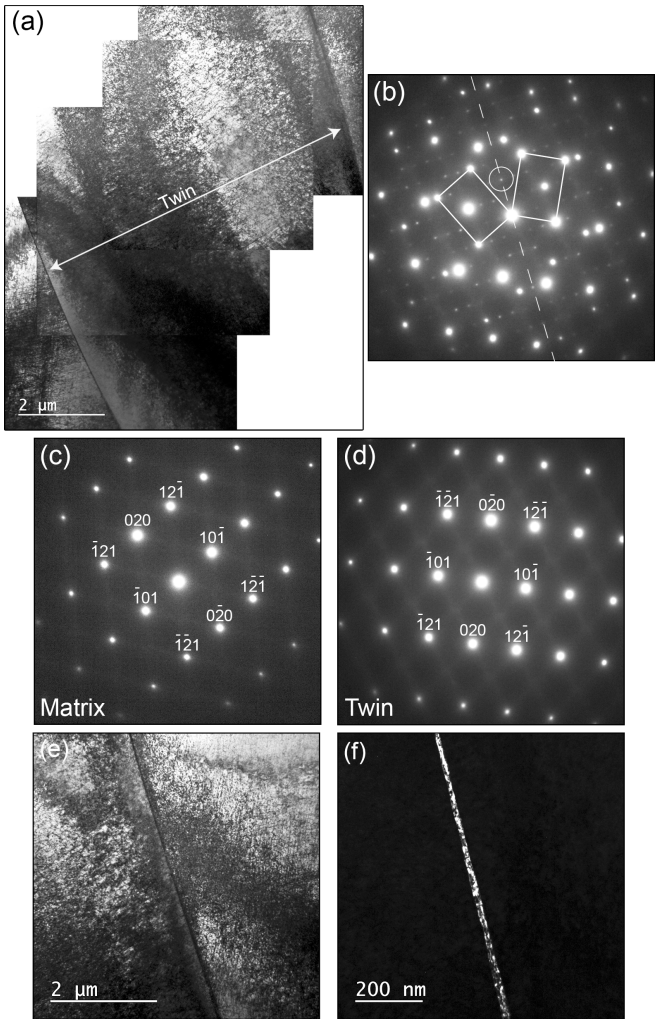


FIG. 3. TEM observations of twin after deformation: (a) Bright field image and (b) corresponding diffraction pattern. (c) Diffraction patterns of matrix and (d) twin only. (e) Focus on the twin boundary and (f) corresponding dark field image taken with the spot encircled in (b).

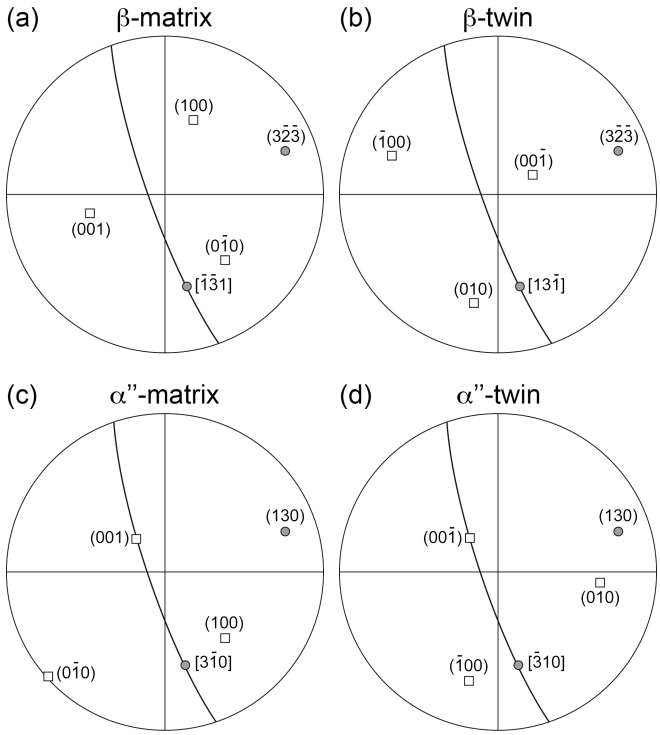


FIG. 4. Stereographic projections of (a) the matrix and (b) the twin observed in Fig. 3. (c-d) Stereographic projections of the same crystals after crystallographic reconstruction in α" martensite.

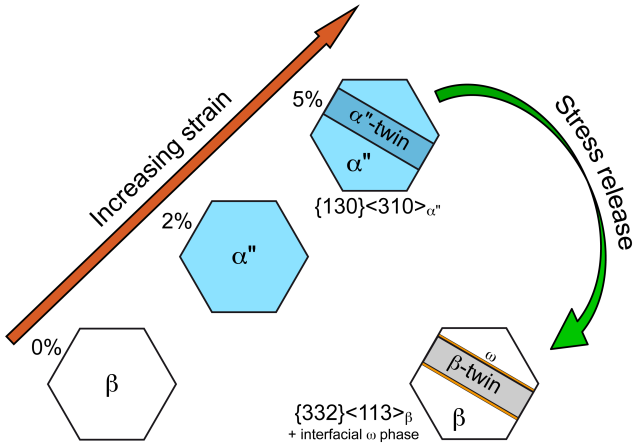


FIG. 5. Schematic formation pathway of {332}<113>$_{\beta}$ twins from the reversion of {130}<310>$_{\alpha"}$ twinning of stress-induced martensite.